symmetry

MDPI

Article

Analysis of Malignant Expansion of Plastic Zone of Surrounding Rocks in High Ground Temperature Hydraulic Tunnels and the Mechanical Characteristics of the Support Structure

Haibo Jiang [1], Yuhang Huang [1], Kebin Shi [2], Pengfei Xiang [1,3,*] and Gang Wei [4,5]

[1] College of Water Conservancy & Architectural Engineering, Shihezi University, Shihezi 832000, China
[2] College of Hydraulic and Civil Engineering, Xinjiang Agriculture University, Urumqi 830052, China
[3] Department of Architectural Engineering, Zhejiang Tongji Vocational College of Science and Technology, Hangzhou 311200, China
[4] Department of Civil Engineering, Zhejiang University City College, Hangzhou 310015, China
[5] College of Civil Engineering and Architecture, Zhejiang University, Hangzhou 310058, China
* Correspondence: z20120190803@zjtongji.edu.cn

Abstract: To explore the development process of the plastic zone of hydraulic tunnels and the mechanical characteristics of the support structure in a high ground temperature environment during construction period, methods, including theoretical analysis, numerical calculation, field monitoring test, etc., are used to analyze the generation and formation process of the plastic zone of surrounding rocks in the hydraulic tunnel under high ground temperature environment. The evolution law of mechanical characteristics of the support structure in surrounding rocks is studied. The development process and shape of the plastic zone in the tunnel under various high ground temperatures are simulated. The results show that after the excavation of the high ground temperature hydraulic tunnel, the plastic zone first appears at the arch waist in a crescent pattern, then extends to both sides and the spandrel, and connects with the plastic zone in the arch crown, forming a pattern of circle or butterfly. A higher initial temperature of the surrounding rock indicates a larger range and plastic strain of the plastic zone in the surrounding rock. At the same time, the plastic zone is easier to appear at the spandrel and arch foot and develop to the depth of the surrounding rock. The higher is the initial temperature of the surrounding rock, the greater will be the axial force and bending moment of supported shotcrete, the more obviously the bending moment of arch abutment and arch foot will grow, the greater will be the axial force value of the bolt and the farther the neutral point will be from the tunnel wall. While strengthening the arch waist, the support of the arch shoulder and arch foot should also be strengthened at a high temperature.

Keywords: high ground temperature; hydraulic tunnel; plastic zone; anchoring support; neutral point

Citation: Jiang, H.; Huang, Y.; Shi, K.; Xiang, P.; Wei, G. Analysis of Malignant Expansion of Plastic Zone of Surrounding Rocks in High Ground Temperature Hydraulic Tunnels and the Mechanical Characteristics of the Support Structure. *Symmetry* **2022**, *14*, 2606. https://doi.org/10.3390/sym14122606

Academic Editor: Sergei Alexandrov

Received: 14 November 2022
Accepted: 5 December 2022
Published: 9 December 2022

1. Introduction

With the tunnel engineering from shallow to deep, the mechanical environment of surrounding rocks in the tunnel becomes increasingly complicated. The deep high ground temperature and high geostress tunnel shows a series of engineering responses such as large-scale surrounding rock failure and complex shape of the plastic zone [1–3]. Both theory and practice have proved that the shape and range of the plastic zone of surrounding rocks in the tunnel is not only an important factor affecting the stability of the tunnel, but also an essential basis for the design of the tunnel support structure.

Researchers have long performed in-depth research on the elastoplastic problem of surrounding rocks in high ground temperature underground tunnels, and obtained fruitful valuable results. Under a high ground temperature environment, the coupling effect of a high ground temperature and high geostress leads to the weakening of surrounding

rock strength, and the expansion of plastic zones further aggravates the development of large squeezing deformation [4]. Bian et al. [5,6] introduced the plastic strain softening characteristics and shear dilation characteristics of surrounding rock into the elastoplastic solution of circular tunnel, and analyzed the influencing factors of the plastic zone in surrounding rock. Lee and Pietruszczak [7] used the numerical difference method to derive the analytical solution of the mechanical response of surrounding rock considering plastic softening. Wang et al. [8–12] deduced and solved the mechanical response of surrounding rock after the excavation of deep-buried tunnel by using the method of Lee and Pietruszczak. They also revealed the failure mechanism of large squeezing deformation in deep-buried tunnels. In the stress path under the complex excavation disturbance of high ground temperature and high geostress, the mechanical response of multi-scale structural rock mass is more complicated. Different scales and degrees of engineering damages may occur at the rock mass near the fault zone, such as the plastic extrusion tensile failure and structural stress collapse, which can lead to the failure of anchor bolt and cable supporting [13–16]. Kim [17], Tremblay [18], and Charlie [19] pointed out that under the load effect, the bonding strength of the interface plays a role first. With the increase of load, the bonding strength of the interface becomes less than the pull-out load, and the first interface begins to appear shear and slip failures. Chen et al. [20] established a shear stress-displacement nonlinear constitutive model that can reflect the mechanical characteristics of bonding-softening-sliding of the anchor bolt interface, and solved the problem that the trilinear softening interface model needs to be analyzed in sections.

Many researchers have studied the characteristics of the plastic zone and the mechanical properties of the support structure in tunnels with high ground temperature using the methods of theoretical analysis, numerical simulation and physical tests. However, at present, there is little research on the dynamic development process and control technology of the plastic zone in the surrounding rock, and a lack of research on systematic theory and support control technology. Therefore, through field monitoring tests, this study analyzes the main characteristics of tunnel deformation and failure, investigates the dynamic development process of the tunnel plastic zone under temperature effect based on theoretical analysis and numerical simulation, and finds the sensitive part to control the tunnel plastic zone. On this basis, the variation characteristics of the plastic zone in the tunnel under temperature effect are emphatically studied, the evolution mechanism of mechanical properties of the support structure for surrounding rocks is analyzed, and the development process and shape of the plastic zone during tunnel supporting are simulated. There are a lot of symmetries in the malignant expansion of the surrounding rock plastic zone and the mechanical properties of the support structure of the high temperature hydraulic tunnel.

2. Field Monitoring Test of High Ground Temperature Hydraulic Tunnel

2.1. Experimental Scheme

This study takes a 4.1 km long tunnel section with high ground temperature in a hydraulic tunnel in Xinjiang as the research object. The tunnel is constructed by drilling and blasting method. The lithology of the rock mass is mica quartz schist sandwiched with graphite schist. The tunnel is dry with no groundwater leakage. The thickness of the overlying strata of the tunnel is approximately 560 m and the tunnel adopts longitudinal ventilation to reduce the temperature inside the tunnel. The high ground temperature area caused by uneven heat conduction has a high temperature and wide scope. During the tunneling process, the maximum ambient temperature at the heading face reached 77 °C, and the maximum temperature of the thermometer hole reached 105 °C. The geographical location of the tunnel is shown in Figure 1. The profile diagram of the tunnel is shown in Figure 2.

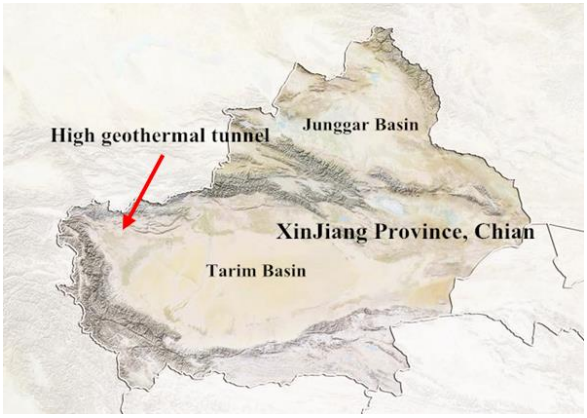

Figure 1. The geographical location of the tunnel.

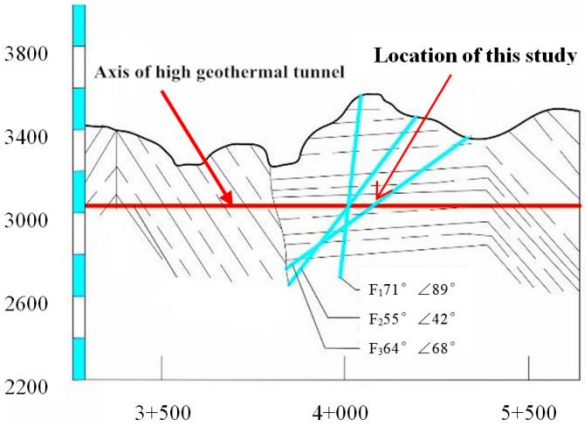

Figure 2. The profile diagram of the tunnel.

When the temperature is monitored, two test sections are set up in the test tunnel (the first 2-m section is the coarse tunnel while the last 3-m section is the concrete sprayed layer). Temperature-measuring hole 1# is located in the section of coarse tunnel, and 2# is located in concrete sprayed section with wire mesh. Four measuring points are set up at 0.5 m, 1.5 m, 2.5 m and 3.5 m from the tunnel wall in each section. The specific layout is shown in Figure 3 as below. In order to guarantee the reliability of the instrument and line, the temperature probe and high temperature cable after special treatment are adopted.

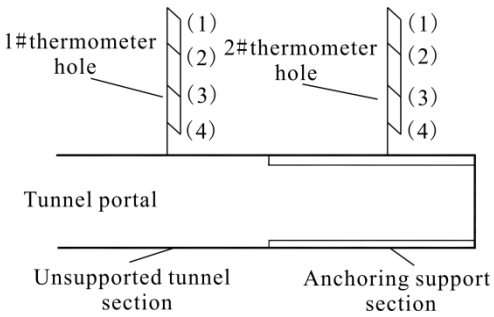

Figure 3. Schematic diagram of temperature monitoring in the test tunnel.

During the stress monitoring of the anchor bolt and spray layer, the spray layer section with hang net was supported by ordinary shotcrete and steel mesh. The steel mesh was composed of Φ8 rebar, and the grid size was 200 × 200 mm. The steel mesh was close to the initial spray surface and welded to the end of the anchor bolt to ensure the stability of the steel mesh during shotcreting. In the primary supporting, C30 concrete with the

impermeability grade of W8 was used, and the thickness of the spray layer was 150 mm. At this period, primary spraying and secondary spraying were conducted. The primary spraying thickness was approximately 50 mm, and the secondary spraying was carried out after the installation of anchor bolts and hanging nets. After the primary spraying is completed, GPL-2 stress gauges for the spray layer were set at the arch top and sidewall of the test tunnel to monitor the circumferential and radial stress of the spray layer. GML stress gauges were installed at 0.5 m, 1.0 m, and 1.5 m of the anchor bolt at the left side and arch top to obtain the axial force data of the anchor bolt. The specific layout is shown in Figure 4.

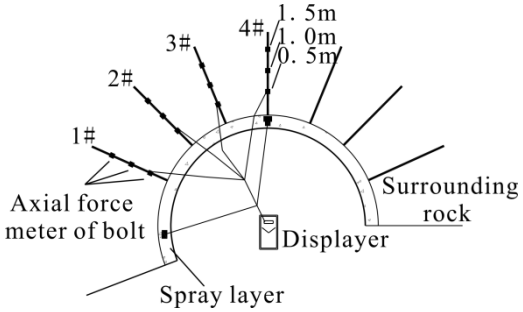

Figure 4. Layout of stress gauges at the anchor bolt and the spray layer.

2.2. Analysis of Monitoring Results

2.2.1. Temperature Distribution Law

The monitoring temperature at each point of the surrounding rock during construction is shown in Figure 5. The temperature changes are basically the same as that between the section of coarse tunnel and the wire mesh sprayed layer as the time goes. With cooling measures, such as ventilation and watering in the early stage, the temperature at each measuring point fell rapidly. In the later stage, the temperature of each measuring point was repeated due to intermittent ventilation cooling. The maximum temperature in the section of coarse hole is 62.8 °C, which is lower than that in the section of mesh spraying at 69 °C. The temperature at each measuring point of coarse hole is lower than that in the mesh sprayed layer at the same time and at the same position. This is because the capacity of heat dissipation in the sprayed concrete mesh falls, and cement hydration of the mesh shotcrete layer will also give off heat. The trend of temperature change is basically the same between different measuring points of the same borehole. The farther is the cave wall, the higher will be the surrounding rock temperature. On the contrary, the closer the wall, the lower the surrounding rock temperature.

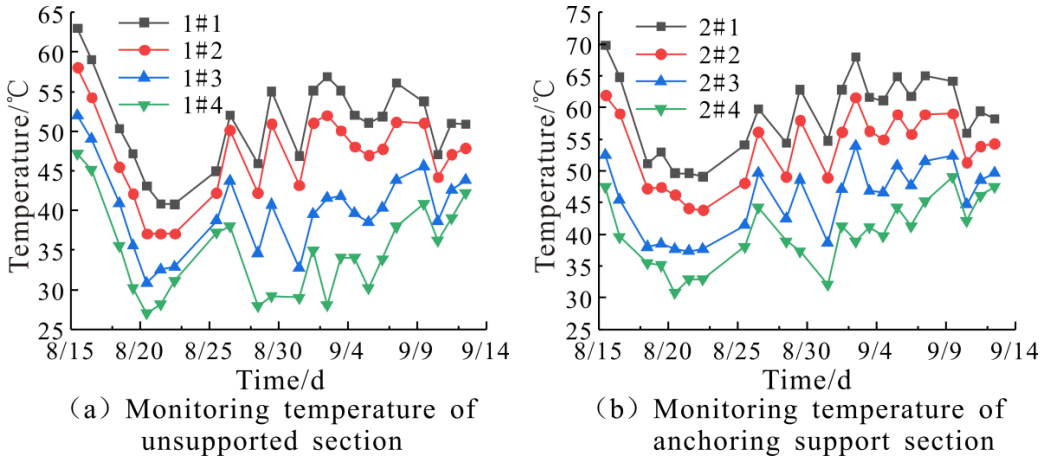

Figure 5. This is a figure. Schemes follow the same formatting.

2.2.2. Stress Distribution Law of the Spray Layer

The monitoring stress values of the spray layer during construction are shown in Figure 6, where positive value represents compressive stress and negative value represents tensile stress.

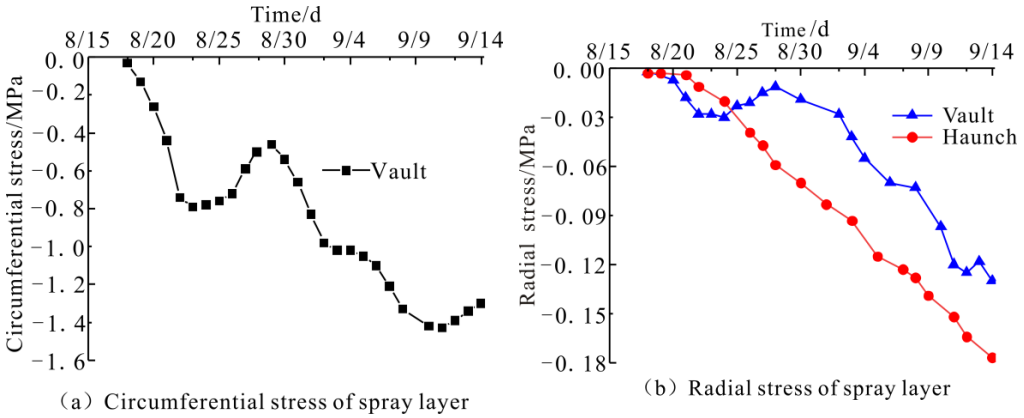

Figure 6. Monitoring values of circumferential and radial stresses of the spray layer.

The circumferential stress and radial stress of sprayed layer tunnel are always tensile stress. During the whole construction, the vault circumferential stress showed a growing trend overall with the maximum value of 1.48 MPa. The vault circumferential stress is repeated, which is possibly associated with the temperature change of surrounding rock. The radial stress at the arch waist of the concrete spayed layer is slightly smaller than that at the vault in the early stage. Since 25 August, the radial stress at the arch waist was always greater than that at the vault. The maximum value of vault radial stress was 0.14 MPa and 0.18 MPa at the arch waist, which were far less than the circumferential stress at the same time.

2.2.3. Distribution Law of Axial Force of the Anchor Bolt

Figure 7 shows the axial force at 0.5 m, 1 m, and 1.5 m of the anchor bolt during construction. The axial force of each anchor bolt is the pulling force. From the figure, the axial force increases with time, and the slope of the curve decreases gradually, indicating that the growth rate of the axial force of each anchor bolt gradually slowed down. The maximum axial force of 1# anchor bolt was at the front end of the anchor bolt (near the end of the tunnel wall), and the maximum axial force was 19.8 kN. The maximum axial force of 2# anchor bolt was in the middle of the anchor bolt, and the maximum axial force was 17.3 kN. After 25 August, the axial force at the front end of the bolt almost no longer increased, indicating that the relative displacement of this bolt and the surrounding rock has been completed, and there was no trend of relative displacement. The overall axial force of 3# and 4# anchor bolts was relatively closer, and their maximum axial force was 13.7 kN and 12.8 kN, respectively. The axial force at the front end of the anchor bolt was much smaller than the overall axial force, and the axial force at the rear end of the anchor bolt did not change significantly.

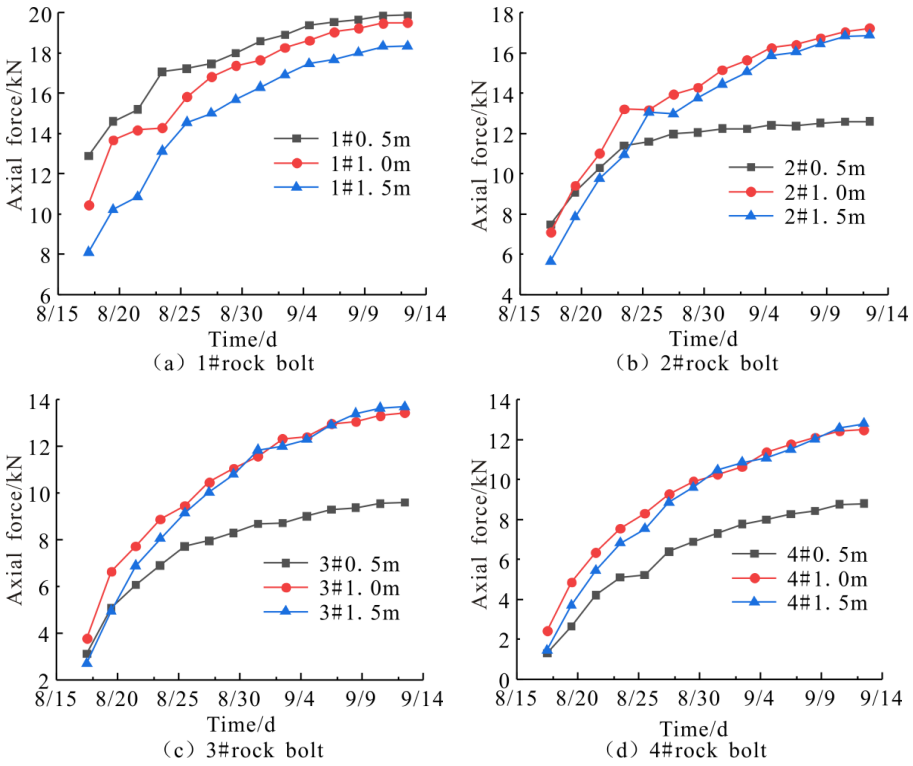

Figure 7. Monitoring axial force of the anchor bolt.

3. Characteristics of Plastic Zone in Surrounding Rocks and Mechanical Properties of the Support Structure in High Ground Temperature Tunnels

3.1. Establishment of Finite Element Model

The buried depth of the high ground temperature hydraulic tunnel is approximately 250 m. Based on the analytical calculation results after the excavation of the circular hydraulic tunnel, its influence range was three to five times the tunnel diameter. The range of the surrounding rock was preliminarily calculated as four times the tunnel diameter from the upper, lower, left, and right side, respectively. On that basis, a finite element backwash model of the high ground temperature tunnel was established, as shown in Figure 8. First, the indirect coupling simulation method was used to calculate the transient temperature field of the model. Then, the results of the transient temperature field were applied to the structural analysis as body load to realize the temperature-stress coupling simulation.

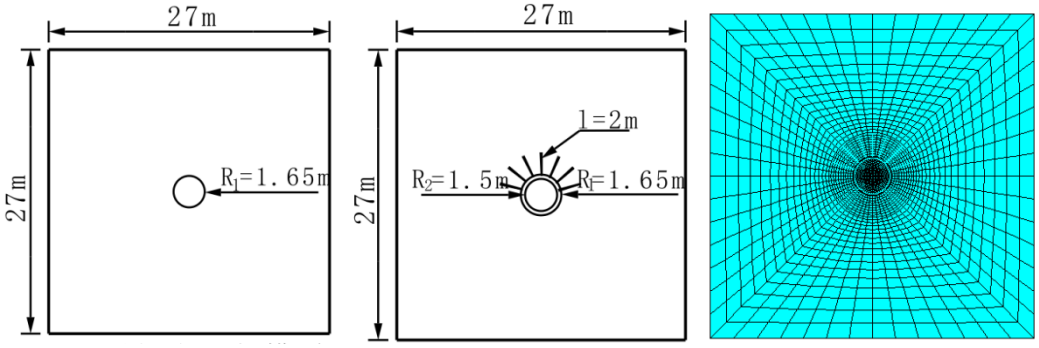

Figure 8. Geometry and finite element model of the tunnel.

The finite element model was established based on the actual situation of the project. Specifically, the diameter of the unsupported tunnel was 3.3 m, the calculated range of surrounding rock was 27 m × 27 m, and the thickness of the spray layer at the spray layer section with hang net was 0.15 m. C30 concrete was used, and HRB335 steel bars were

used for the anchor bolt. The length of the bolt was 2 m, and the diameter was 25 mm. The bonding material was the M20 cement mortar. The geometric model and numerical model of the unsupported tunnel section and the spray layer section with hang net are shown in Figure 8. The element birth and death technique was used to deal with the anchor bolt and spray layer elements in the simulation of the unsupported tunnel.

According·to the engineering actual situation, ventilation was conducted after the excavation of the tunnel, and the wall boundary of the model was the convection heat transfer boundary. Field monitoring data showed that the temperature of ventilation air was approximately 20 °C. The convection heat transfer coefficient between the tunnel wall and the air was 30 $W\cdot(m^2\cdot{}^\circ C)^{-2}$, while the convection heat transfer coefficient between the spray layer and the air was 45 $W\cdot(m^2\cdot{}^\circ C)^{-2}$.

3.2. Selection of Thermodynamic Parameters

According to the analysis of the field measured data, the density of the surrounding rock was 2650 kg/m^3, the tensile strength was 1.4 MPa, the compressive strength was 40.85 MPa, the internal friction angle was 37°, the cohesion force was 1.1 MPa, the elastic modulus was 7.1 GPa, and the Poisson's ratio was 0.28. At room temperature, the thermal conductivity of the surrounding rock was 15 $W\cdot(m^2\cdot{}^\circ C)^{-1}$, the linear expansion coefficient was 5×10^{-6} $^\circ C^{-1}$, and the specific heat capacity was 1060 $J\cdot(kg\cdot{}^\circ C)^{-1}$. According to the literature [15–17], the mechanical parameters of surrounding rock at different temperatures were calculated, and the results are listed in Table 1.

Table 1. Mechanical parameters of the surrounding rock at different temperatures.

Temperature/°C	Thermal Conductivity/W·(m·°C) $^{-1}$	Linear Expansion Coefficient/10^{-6} °C^{-1}	Specific Heat Capacity/J·(kg·°C)$^{-1}$	Elastic Modulus/GPa	Poisson's Ratio
20	15	5	1060	7.1	0.28
30	14.37	5.4	1090	7.1	0.269
40	13.79	5.8	1120	7.09	0.276
50	13.25	6.2	1150	7.07	0.282
60	12.75	6.7	1180	7.04	0.289
70	12.29	7.2	1210	7.01	0.295
80	11.87	7.6	1240	6.97	0.302

The concrete density was 2550 kg/m^3, the Poisson's ratio was 0.167, the compressive strength was 15 MPa, and the tensile strength was 1.5 MPa. According to the literature [18–21], other mechanical parameters of concrete at different temperatures were calculated, as shown in Table 2.

Table 2. Mechanical parameters of the concrete at different temperatures.

Temperature/°C	Thermal Conductivity/W·(m·°C)$^{-1}$	Linear Expansion Coefficient/10^{-6} °C^{-1}	Specific Heat Capacity/J·(kg·°C)$^{-1}$	Elastic Modulus/GPa
20	1.69	6.16	913	30.00
30	1.67	6.24	920	28.20
40	1.65	6.32	926	27.78
50	1.64	6.40	933	27.36
60	1.62	6.48	939	26.94
70	1.60	6.56	945	26.52
80	1.59	6.64	952	26.10

3.3. Analysis of Temperature Simulation Results

Different initial boundary temperatures were set to perform simulation analysis on the transient thermal mechanical coupling for the unsupported tunnel section and the spray layer section with hang net after excavation. When the initial temperature was 80 °C, the simulation value of surrounding rock temperature was consistent with the measured value.

Figure 9 shows the temperature of surrounding rocks in the unsupported tunnel section and the spray layer section with hang net after 5 days of excavation. Figure 10 compares the measured temperature and the simulated temperature of surrounding rocks in the unsupported tunnel section and the spray layer section with hang net at the initial stage of construction.

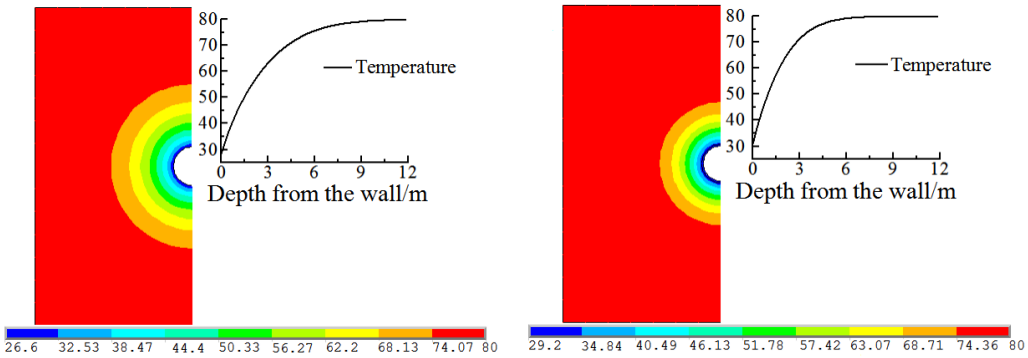

(**a**) Unsupported tunnel section (**b**) Spray layer section with hang net

Figure 9. Temperature contours of the unsupported tunnel section and the spray layer section with hang net (°C).

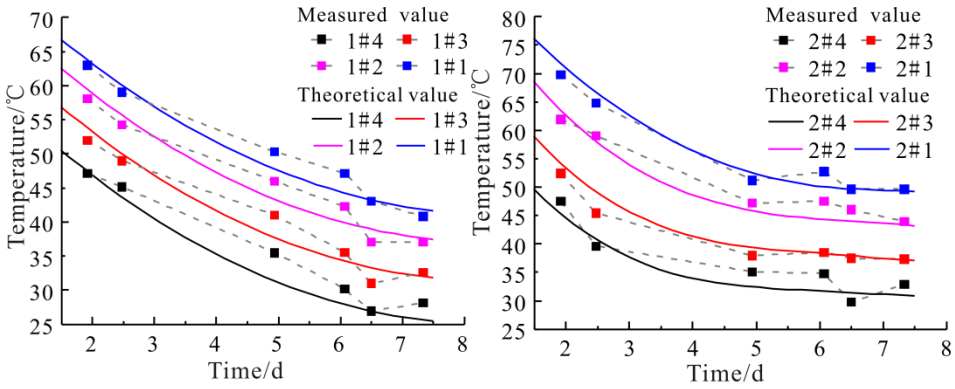

(**a**) Unsupported tunnel section (**b**) Spray layer section with hang net

Figure 10. Comparison curve of the measured and simulated temperatures of surrounding rocks at the initial stage of construction.

After excavation, the temperature variation radius of the surrounding rock in the unsupported tunnel section was larger than that of the spray layer section with a hang net in the same period, and at the same distance from the tunnel wall, the temperature of the spray layer section with hang net was higher than that in the unsupported tunnel section. This indicates that the heat release rate of surrounding rock in the unsupported tunnel section was faster than that in the spray layer section with hang net, and the spray layer had a certain thermal insulation effect after the anchoring support.

From Figure 10, the temperature curve of the coupling simulation has the same variation trend as the measured temperatures at each point, that is, the temperature decreased with time after excavation. The temperature decreased rapidly at the beginning of excavation, and then the dropping rate gradually slowed down. There existed differences between the simulated temperature and the measured temperature, and the maximum difference was only 7%, which was within a reasonable range.

The on-site temperature monitoring results verified that the mechanical parameters of the surrounding rock and the concrete selected for numerical simulation were appropriate and can be used for subsequent coupling simulation analysis.

3.4. Evolution Law of Plastic Zone Characteristics of Surrounding Rock at Different Stages

The initial temperature of surrounding rock was set as 80 °C, the node temperature by transient thermal simulation was applied as the body load to the structural analysis, and the element birth and death technique was used to conduct the simulation analysis of the tunnel excavation. At this time, in order to simulate the distribution characteristics of the plastic zone in surrounding rocks of the supported tunnel after excavation, no follow-up supporting was carried out.

The development of the plastic zone after tunnel excavation is shown in Figure 11. After excavation, the stress was gradually released, and the plastic zone appeared first at the arch waist. After the excavation for 1 day, the maximum plastic strain value was 0.0012, and the thickness of the plastic zone was approximately 0.32 m. After 5 days of excavation, the plastic zone was further expanded. To be specific, the plastic zone at the arch waist on both sides expanded upward and downward, and connected with the plastic points at the arch crown and arch bottom, developing into a "circle" plastic zone. The plastic strain value increased by 50%, and the thickness of the plastic zone was 0.4 m. At the 10th day of excavation, the maximum plastic strain increased less than that at the 5th day of excavation, reaching only 0.0019. However, the plastic zone at the spandrel showed an obviously extension to the depth of the spandrel, and the thickness of the plastic zone was 1 m. At the same time, the thickness of the plastic zone at the arch waist was approximately 0.48 m. On the whole, the plastic zone of surrounding rocks exhibited a "butterfly" pattern, which was consistent with the conclusion in the literature [22,23].

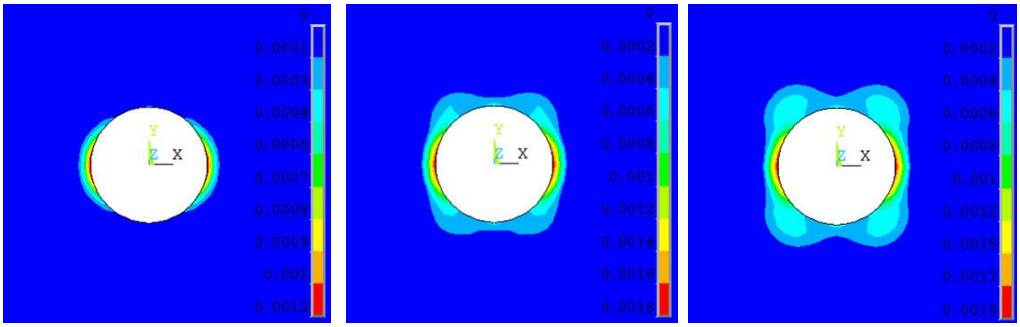

(**a**) 1 day after excavation (**b**) 5 days after excavation (**c**) 10 days after excavation

Figure 11. Plastic zone after 1 day, 5 days, and 10 days of excavation.

To effectively limit the development of the plastic zone at the arch crown and spandrel, the supporting time should be not too early. Because the too early supporting cannot fully utilize the self-supporting capacity of the surrounding rock [24]. Therefore, the supporting time was selected on the 2nd day after the excavation. After 10 days of excavation, the plastic strain value of each area reached the maximum, and the plastic zone was basically unchanged. Then, the plastic zone formed after 10 days of excavation was regarded as the final plastic zone caused by excavation.

3.5. Mechanical Characteristics of the Surrounding Rock and the Anchor Bolt in the Spray Layer Section with Hang Net

The surrounding rocks around the bolt were simplified as homogeneous, continuous, and isotropic ideal elastoplastic bodies. The damage of the bolt to the surrounding rock structure was ignored, no relative sliding occurred, and the tensile strength of the bolt was much greater than that of the surrounding rock. The initial temperature was set at 80 °C, and the spray layer section with hang net was simulated. According to the development of the plastic zone in the unsupported tunnel section after the excavation, the anchoring support was carried out 2 days after the excavation.

3.5.1. Distribution Law of the Axial Force of the Anchor Bolt

The fully grouted anchor prevents the deformation of surrounding rock by the cohesive force or friction between the bolt and the bonding material. After the bolt was adopted, the surrounding rock near the cavern space moved towards the interior of the excavated tunnel. The bolt prevented the surrounding rock from moving, at this moment, the bolt surface was subject to the shear force pointing to the tunnel. In the deep surrounding rock far away from the cavern, the displacement of the anchorage body was larger than that of the surrounding rock mass, and the shear stress between the anchorage body and the surrounding rock mass pointed away from the tunnel. Since the shear force at both ends of the bolt are opposite, there must be a point on the bolt body where the shear forces at the left and right sides are opposite, which is called as "Neutral Point" [25]. The approximate location of the "Neutral Point" can be determined by the maximum axial force in the simulation results. The axial force of bolt changes as shown in Figure 12.

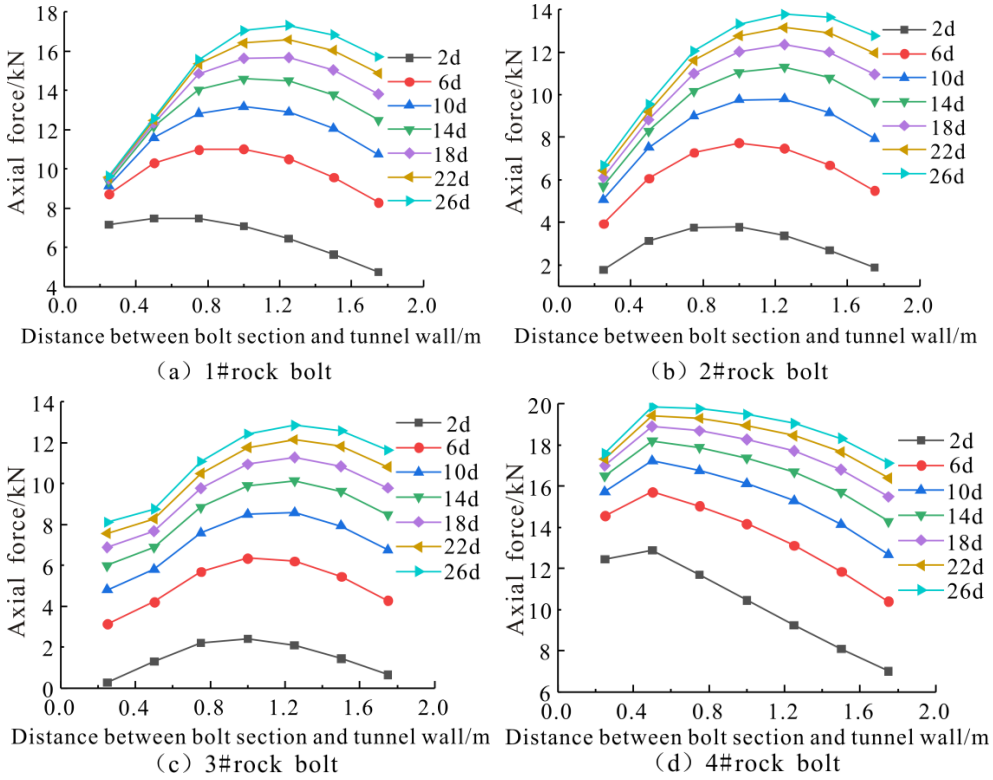

Figure 12. Variation curve of the axial force of the anchor bolt.

The axial force of the rod rose firstly and then fall along the depth of which the rod pointed to the surrounding rock, and the axial force between the rods was greater than that at both ends. The maximum axial force of bolt at different angles was different at the same moment. The maximum axial force of Anchor 1# is at 0.6 m, that of Anchor 2# and 3# is at 0.8 m, and that of Anchor 4# is at 0.5 m. The neutral point of bolt in different position at the same moment is different. Except the top of the arch, the closer the neutral point of the bolt is near the top arch, the farther the tunnel wall will be. On the contrary, it will be closer to the tunnel wall. The maximum axial force of the same bolt is different at different moments. As anchor time goes, the maximum axial force point of 1#~3# moves off the tunnel wall, while the neutral point moves away from the tunnel wall. After anchor supported, the surrounding rock stress will still be released with the time, the displacement and plastic zone will continuously expand. In order to limit the growth of the surrounding rock displacement, the shear force between the bolt surface and the surrounding rock grow gradually, so does the axial force at each point of the bolt. The change of "Neutral Point" and axial force with the time can be seen in Figure 13.

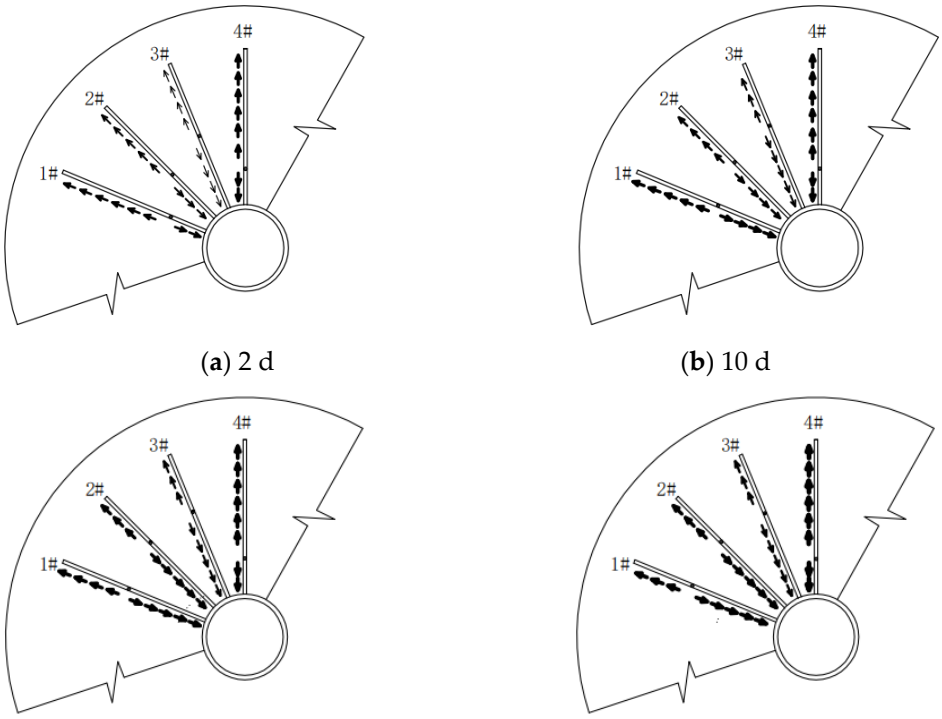

(**a**) 2 d (**b**) 10 d

(**c**) 18 d (**d**) 26 d

Figure 13. Change of anchor "Neutral Point" and axial force with time.

3.5.2. Changes of Plastic Zone in Surrounding Rocks after Anchoring Support

The maximum plastic strain after 3 days of supporting was 0.0011, and the maximum plastic strain after 8 days of supporting was 0.0014, increasing by 27.3%. During the same period, when the tunnel was unsupported, the maximum plastic strain was 0.0018 and 0.0019, respectively. The plastic zone of the anchoring part had significant variations compared with that of the unanchored part. The maximum plastic strain decreased by 38.9% and 26.3%, respectively, and the range of the plastic zone decreased by 29% and 20%, respectively. After the supporting, the deformation rate of the plastic zone in surrounding rocks dropped, indicating the anchoring support had an obvious restriction on the development of the plastic zone in high ground temperature surrounding rocks, as shown in Figure 14.

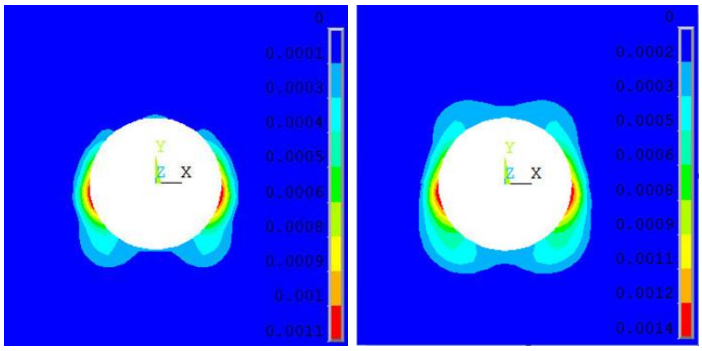

(**a**) 3 days after supporting (**b**) 8 days after supporting

Figure 14. Distribution of Plastic Zone in Surrounding Rocks after 3 and 8 Days of Supporting.

3.6. Mechanical Characteristics of the Surrounding Rock and Support Structure at Different Temperatures

In order to explore the mechanical characteristics of the surrounding rock and support structure under different temperatures, the initial simulation temperatures were set at

20 °C, 50 °C, 80 °C. The distribution of the plastic zone in surrounding rock and the mechanical characteristics of anchor support structure under different initial temperature were simulated and analyzed.

3.6.1. Plastic Zone of the Unsupported Tunnel under Different Initial Temperatures

Figure 15 shows the distribution of the plastic zone after 12 days of excavation at different initial temperatures. The maximum plastic strain of surrounding rock occurred at the arch waist. A higher initial temperature of surrounding rock indicates larger plastic zone area and larger plastic strain value. When the temperature was 20 °C, the thickness of the plastic zone was 0.3 m, and the plastic zone was distributed at both sides of the arch waist in a "crescent" pattern. When the initial temperature was 50 °C, the maximum plastic strain was 0.0016, increasing by 78% compared with that at 20 °C, and the plastic zone extended to the spandrel and arch foot in the upper and lower sides. At the same time, plastic points began to appear at the arch crown and arch bottom. When the initial temperature was 80 °C, the maximum plastic strain was 0.0019, increasing by 111% compared with that at 20 °C. An obvious extension trend of the plastic zone to the depth appeared at the spandrel and arch foot, and the thickness reached 1.2 m. Meanwhile, the thickness of the plastic zone at the arch waist was 0.5 m.

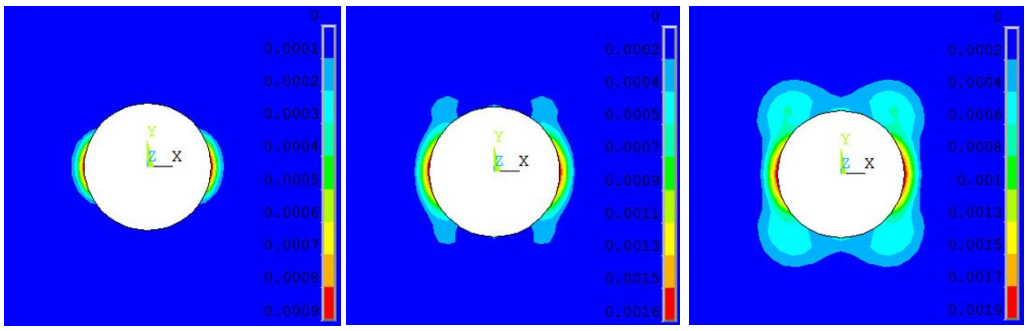

(**a**) 20 °C (**b**) 50 °C (**c**) 80 °C

Figure 15. Development process of the plastic zone in surrounding rocks at different initial temperatures after 12 days of excavation.

A higher initial temperature of surrounding rock indicates a larger plastic zone of surrounding rock and a larger maximum plastic strain. When the temperature was 80 °C, the plastic zone at the spandrel and arch foot had an obvious malignant development towards the depth of surrounding rock. Therefore, compared with tunnel excavation in normal temperature, after the excavation in a high ground temperature environment, it is more necessary to conduct anchoring support on the free face under the combined action of surrounding rock stress redistribution and temperature stress, and appropriately adjust the strength and form of the support structure. The higher the temperature, the more attention should be paid to the anchoring support at the spandrel and arch crown.

3.6.2. Plastic Zone of Surrounding Rock after Anchoring Support

Figure 16 shows the plastic zone of surrounding rock after anchoring support for 10 days under different initial temperature environments. From the figure, the plastic zone of the anchoring part has significant changes compared with that of the unsupported part in the same period. When the initial temperature was 20 °C, the maximum plastic strain value after 10 days of supporting was 0.0007, reducing by 22.2% compared with that of the unsupported part in the same period, and the plastic zone area decreased by 9% compared with that in the same period. When the initial temperature was 50 °C, the maximum plastic strain value of surrounding rock was 0.0013, reducing by 27.8% compared with that of the unsupported part in the same period, and the area of the plastic zone decreased by 20%. When the initial temperature was 80 °C, the maximum plastic strain value was 0.0015,

reducing by 21.1% compared with that of the unsupported part in the same period, and the area of the plastic zone decreased by 24%. After anchoring support, the plastic strain value and plastic zone area of surrounding rocks were significantly reduced, which indicates that the anchoring support can limit the development of the plastic zone of high-temperature surrounding rocks. The higher the initial temperature, the more obvious the effect of the support structure.

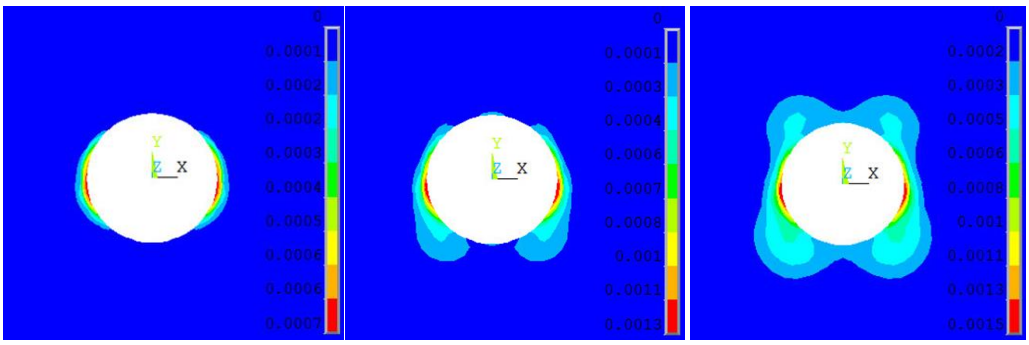

(**a**) 20 °C (**b**) 50 °C (**c**) 80 °C

Figure 16. Plastic zone after 10 days of supporting at different initial temperatures.

3.6.3. Mechanical Characteristics of the Spray Layer

Figures 17–19 show the bending moment and axial force of the spray layer after 10 days of supporting at different initial temperatures. When the initial temperature was 20 °C, the maximum bending moment of the spray layer was 1.52 kN·m, which was located at the arch waist, and the outside was subject to tension forces. At the same time, the maximum axial force of the spray layer at the arch waist was 479 kN, which was under compression. This shows that the surrounding rock stress by the spray layer at the arch waist was greater than that in other areas, which was consistent with the maximum compressive stress at the arch waist after the tunnel excavation. In the other parts, the bending moment was subjected to tension forces inside. The bending moment at the arch crown and arch bottom area was smaller, and the axial force was smaller than that of other areas. When the initial temperature was 60 °C, the bending moment at the arch waist increased to 1.62 kN·m, the tensile area outside the spray layer expanded from the arch waist to the spandrel, and the tension at the arch foot changed from the internal tension at 20 °C to the external tension. The bending moment values in other parts were all higher than those at 20 °C, and the increase in bending moment at the arch bottom was more obvious than that at the arch crown. The spray layer was under pressure as a whole, and the axial force increased compared with that at 20 °C. The maximum axial force at the arch waist was 1110 kN, and the axial stress of the spray layer at the arch waist was 7.4 MPa. When the initial temperature was 80 °C, the bending moment of the spray layer showed obvious variations. Specifically, the bending moment of the spray layer at both sides of the arch waist and the upward and downward extension area was subjected to tension forces outside, while the spray layer at the arch crown and arch bottom was subjected to tension forces inside. The bending moment subjected to tension forces inside increased faster, and the maximum bending moment was at the arch bottom.

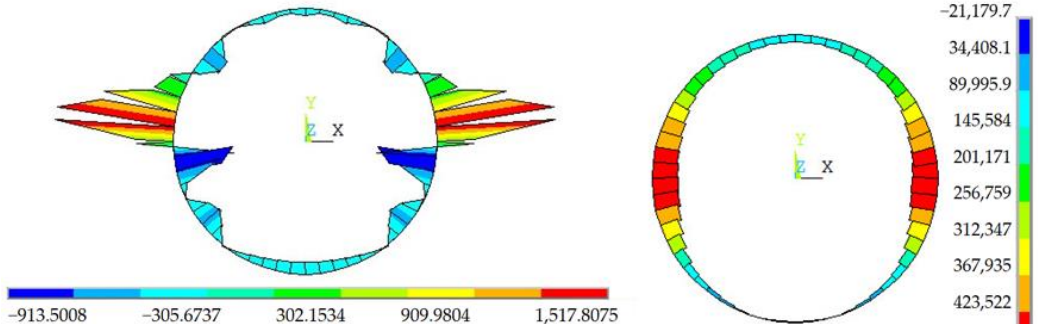

Figure 17. Bending moment (N·m) and axial force (N) of the spray layer after 10 days of supporting at 20 °C.

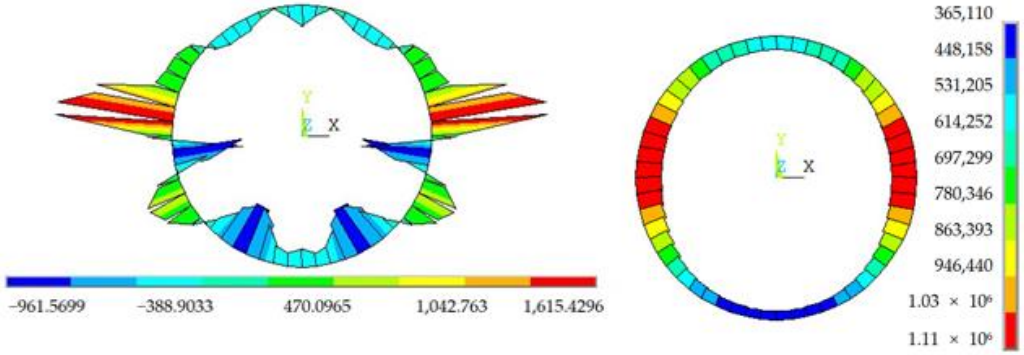

Figure 18. Bending moment (N·m) and axial force (N) of the spray layer after 10 days of supporting at 50 °C.

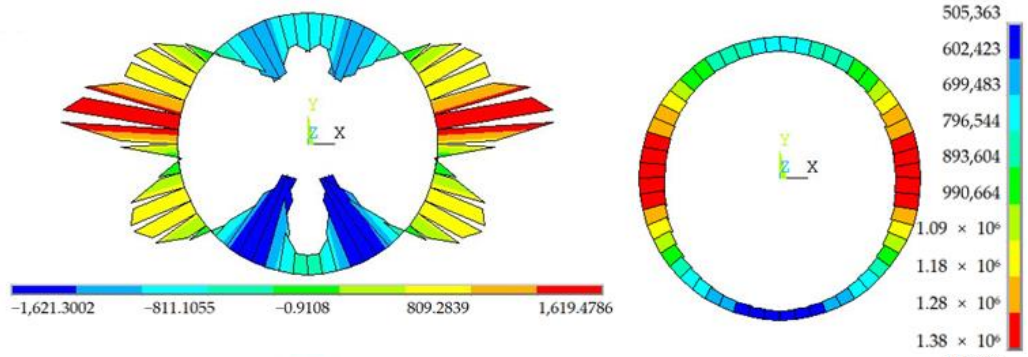

Figure 19. Bending moment (N·m) and axial force (N) of the spray layer after 10 days of supporting at 80 °C.

3.6.4. Axial Force of the Bolt at Different Temperatures

Figure 20 shows the axial force of the anchor bolt under different initial surrounding rock temperatures. From the figure, the axial force of 1#, 2#, and 3# anchor bolts close to the tunnel wall is inversely related to the initial surrounding rock temperature. The lower the temperature, the greater the axial force. This indicates that the higher the growth rate of the axial force, the greater the interface shear stress at the front end of the anchor bolt, which is consistent with the theoretical analysis results above. Far away from the tunnel wall, the axial force of the anchor bolt is positively related to the temperature, and the higher the temperature, the greater the changes of the axial force along the anchor bolt. This indicates that the higher the temperature, the greater the effect of the temperature stress caused by the temperature change on the anchor bolt. At the same position (arch crown) of the 4# anchor bolt, the higher the initial surrounding rock temperature, the greater the axial force. The axial force of the anchor bolt increased almost proportionally at different temperatures.

The ratio of the axial force of the anchor bolt at the initial temperatures of 20 °C and 50 °C was smaller than that at the initial temperatures of 50 °C and 80 °C. This indicates that at a higher surrounding rock initial temperature, the temperature effect under the same temperature difference was more obvious, and the effect of the temperature stress on the anchor bolt was greater. At the same location, the higher the temperature of the anchor bolt, the greater the maximum axial force of the anchor bolt, and the farther the distance from the tunnel wall, i.e., the farther away the neutral point from the tunnel wall. During the actual engineering anchoring, the size and strength of the anchor bolt can be reasonably adjusted according to the surrounding rock temperature. Scheme diagram for the "Neutral Point" and the axial force changing with the temperature as in Figure 21.

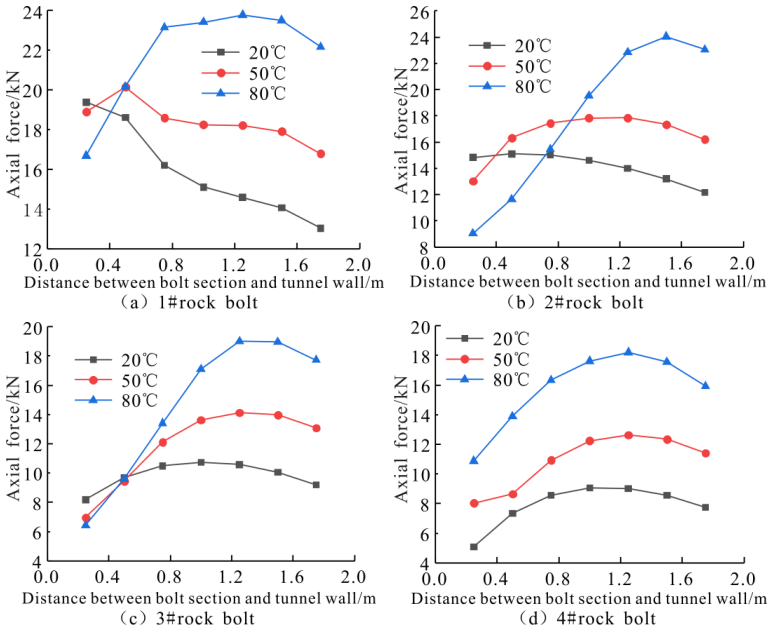

Figure 20. Axial force of the anchor bolt at different temperatures.

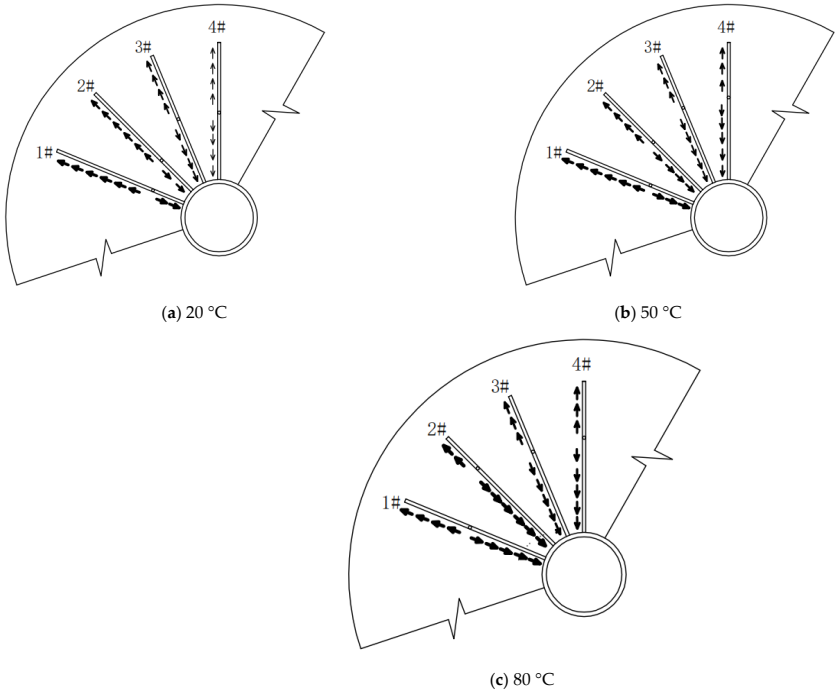

Figure 21. Scheme diagram for the "Neutral Point" and the axial force changing with the temperature.

4. Discussion

(1) After the excavation of the high ground temperature hydraulic tunnel, the plastic zone first appeared at the arch waist in a "crescent" shape, then extended to both sides and the spandrel, and connected with the plastic zone in the arch crown, forming a pattern of a circle or butterfly. When the initial temperature was 50 °C and 80 °C, the maximum strain values of the plastic zone were 0.0016 and 0.0019, respectively, increasing by 76% and 111% compared with that at 20 °C. The higher the initial temperature of the surrounding rock, the larger the range and plastic strain of the plastic zone in surrounding rocks. The plastic zone at the spandrel and arch foot developed malignantly towards the depth of surrounding rock;

(2) The neutral points of bolts at different positions are different at the same moment. Other than the arch top, the closer the neutral point of the anchor is to the arch, the farther it will be from the tunnel wall. On the contrary, it will be closer to the tunnel wall. The axial force of the bolt grows gradually with the time, and the growing speed become smaller gradually until it tends to be stable and does not grow. The neutral point moves toward first and then off the wall;

(3) The higher is the initial temperature of the surrounding rock, the greater will be the axial force and bending moment of the supported sprayed layer, the greater the surrounding rock load and the temperature stress will be; the higher the temperature is, the more obviously the bending moment will grow. Therefore, compared with strengthening the support for the arch waist under normal temperature, the support for both arch shoulder and foot should be strengthened.

Due to the high ground temperature, the monitoring data of sprayed layer stress and bolt axial force in hydraulic tunnel are few. It is necessary to collect more data on relevant engineering in the future to verify the reliability of the conclusions made through the numerical calculation and theoretical analysis.

Author Contributions: Methodology and guidance, H.J.; data curation, editing and analysis, Y.H.; supervision and interpretation of data, K.S.; analysis and project administration P.X.; review and revision, G.W. All authors have read and agreed to the published version of the manuscript.

Funding: This research was funded by the Regional innovation Guidance Plan project of the XPCC, grant number 2021BB004; the National Natural Science Foundation of China, grant number 51769031; and the Horizontal Projects of Zhejiang Tongji Vocational College of Science and Technology in 2022, grant number ZJTK2022008.

Institutional Review Board Statement: Not applicable.

Informed Consent Statement: Not applicable.

Data Availability Statement: Not applicable.

Conflicts of Interest: The authors declare no conflict of interest.

References

1. Chen, Y.L.; Ni, J.; Shao, W.; Azzam, R. Experimental study on the influence of temperature on the mechanical properties of granite under uniaxial compression and fatigue loading. *Int. J. Rock Mech. Min. Sci.* **2012**, *56*, 62–66. [CrossRef]
2. Ren, S.; Bai, Y.M.; Zhang, J.P.; Jiang, D.Y.; Yang, C.H. Experimental investigation of the fatigue properties of salt rock. *Int. J. Rock Mech. Min. Sci.* **2013**, *64*, 68–72.
3. Xia, C.C.; Zhou, S.W.; Hu, Y.S.; Zhang, P.Y.; Zhou, Y. Preliminary study on mechanical property of basalt subjected to cyclic uniaxial stress and cyclic temperature. *Chin. J. Geotech. Eng.* **2015**, *37*, 1016–1024.
4. Sun, J.; Pan, X.M. Research on large squeezing deformation and its nonlinear rheological mechanical characteristics of tunnel with weak surrounding rocks. *Chin. J. Rock Mech. Eng.* **2012**, *31*, 1957–1968.
5. Bian, Y.W.; Xia, C.C.; Xiao, W.M.; Zhang, G.Z. Visco-elastoplastic solutions for circular tunnel considering stress release and softening behaviour of rocks. *Rock Soil Mech.* **2013**, *34*, 211–220.
6. Yao, G.S.; Li, J.P.; Gu, S.C. Analytic solution to deformation of soft rock tunnel considering dilatancy and plastic softening of rock mass. *Rock Soil Mech.* **2009**, *30*, 463–467.
7. Lee, Y.K.; Pietruszczak, S. A new numerical procedure for elasto-plastic analysis of a circular opening excavated in a strain-softening rock mass. *Tunn. Undergr. Space Technol.* **2008**, *23*, 588–599. [CrossRef]

8. Wang, S.L.; Yin, X.T.; Tang, H.; Ge, X.R. A new approach for analyzing circular tunnel in strain-softening rock masses. *Int. J. Rock Mech. Min. Sci.* **2010**, *47*, 170–178. [CrossRef]
9. Han, J.X.; Li, S.C. A procedure of strain-softening model for elasto-plastic analysis of a circular opening considering elasto-plastic coupling. *Tunn. Undergr. Space Technol.* **2013**, *37*, 128–134. [CrossRef]
10. Zhang, Q.; Jiang, B.S.; Wang, S.L. Elasto-plastic analysis of a circular opening in strain-softening rock mass. *Int. J. Rock Mech. Min. Sci.* **2012**, *50*, 38–46. [CrossRef]
11. Zou, J.F.; Li, C.; Wang, F. A new procedure for ground response curve(GRC) in strain-softening surrounding rock. *Comput. Geotech.* **2017**, *89*, 81–91. [CrossRef]
12. Xia, C.C.; Xu, C.; Liu, Y.P.; Han, C.L. Elastoplastic solution of deep buried tunnel considering strain-softening characteristics based on GZZ strength criterion. *Chin. J. Rock Mech. Eng.* **2018**, *37*, 2468–2477.
13. Xu, D.P.; Feng, X.T.; Cui, Y.J.; Jiang, Q.; Zhou, H. On failure mode and shear behavior of rock mass with interlayer staggered zone. *Rock Soil Mech.* **2012**, *33*, 129–136.
14. Duan, S.Q.; Feng, X.T.; Jiang, Q.; Xu, D.P.; Xu, H.; Liu, G.F. Experimental study of mechanical properties of staggered zones under loading and unloading conditions of high stresses. *Chin. J. Rock Mech. Eng.* **2016**, *35*, 1090–1101.
15. Duan, S.Q.; Feng, X.T.; Jiang, Q.; Liu, G.F.; Pei, S.F.; Fan, Y.L. In situ observation of failure mechanisms controlled by rock masses with weak interlayer zones in large underground cavern excavations under high geostress. *Rock Mech. Rock Eng.* **2017**, *50*, 2465–2493. [CrossRef]
16. Duan, S.Q.; Jiang, Q.; Xu, D.P.; Liu, G.F. Experimental study of mechanical behavior of interlayer staggered zone under cyclic loading and unloading condition. *Int. J. Geomech.* **2020**, *20*, 04019187. [CrossRef]
17. Kim, T.S.; Sim, B.K.; Lee, K.S.; Lee, I.M. The effect of pressurized grouting on pullout resistance and the group effect of compression ground anchor. *J. Korean Geotech. Soc.* **2010**, *26*, 5–19.
18. Tremblay, P.; Laceyj, R.W.; Leconte, R. The impact of grain orientation and pebble surface roughness on the bond strength of simulated anchor ice. *Cold Reg. Sci. Technol.* **2013**, *96*, 36–44. [CrossRef]
19. Charlie, C. Analysis of inflatable rock bolts. *Rock Mech. Rock Eng.* **2016**, *49*, 273–289.
20. Chen, J.G.; Chen, X.D. Analysis of whole process of bolt pulling based on wavelet function. *Rock Soil Mech.* **2019**, *40*, 4590–4596.
21. Lie, T.T. A procedure to calculate fire resistance of structural members. *Fire Mater.* **1984**, *8*, 40–48. [CrossRef]
22. Wang, W.J.; Guo, G.Y.; Zhu, Y.J.; Yu, W. Malignant development process of plastic zone and control technology of high stress and soft rock roadway. *J. China Coal Soc.* **2015**, *40*, 2747–2754.
23. Ma, N.J.; Zhao, X.D.; Zhao, Z.Q.; Li, J.; Guo, X.F. Stability analysis and control technology of mineroadway roof in deep mining. *J. China Coal Soc.* **2015**, *40*, 2287–2295.
24. Su, K.; Cui, J.P.; Zhang, Z.M. Method of choosing initial supporting time during tunnel excavations. *J. Cent. South Univ. (Sci. Technol.)* **2015**, *40*, 2287–2295.
25. Du, Y.L.; Feng, G.R.; Kuang, H.P.; Zhang, Y.J.; Zhang, X.H. Effects of different pull-out loading rates on mechanical behaviors and acoustic emission responses of fully grouted bolts. *J. Cent. South Univ.* **2021**, *28*, 2052–2066. [CrossRef]